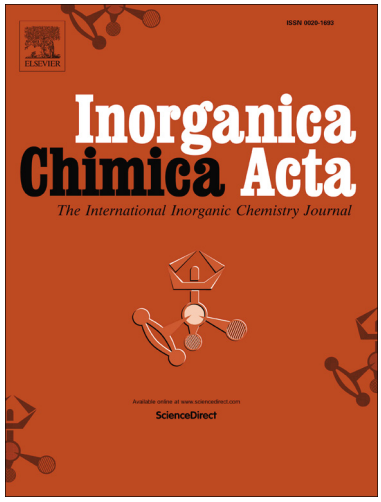

Research paper

Modulation of photophysical properties of copper(I) complexes containing pyridyl-imidazole (PyIm) ligands functionalized by naphthyl, phenanthryl, and anthryl groups

Jinglan Wang, Caoyang Cai, Shengxian Xu, Feng Zhao, Hongying Xia, Yibo Wang

PII: S0020-1693(18)30848-X
DOI: https://doi.org/10.1016/j.ica.2018.09.059
Reference: ICA 18517

To appear in: *Inorganica Chimica Acta*

Received Date: 28 May 2018
Revised Date: 28 August 2018
Accepted Date: 20 September 2018

Please cite this article as: J. Wang, C. Cai, S. Xu, F. Zhao, H. Xia, Y. Wang, Modulation of photophysical properties of copper(I) complexes containing pyridyl-imidazole (PyIm) ligands functionalized by naphthyl, phenanthryl, and anthryl groups, *Inorganica Chimica Acta* (2018), doi: https://doi.org/10.1016/j.ica.2018.09.059

Modulation of photophysical properties of copper(I) complexes containing pyridyl-imidazole (PyIm) ligands functionalized by naphthyl, phenanthryl, and anthryl groups

Jinglan Wang[a] Caoyang Cai[a], Shengxian Xu[a], , Feng Zhao[a] *, Hongying Xia[a] , Yibo Wang[b]

[a] *School of Chemistry and Chemical Engineering, Jiangxi Science and Technology Normal University, Fenglin Street Nanchang, Jiangxi 330013, PR China.*

[b]*Key Laboratory of Guizhou High Performance Computational Chemistry, Department of Chemistry, Guizhou University, Guiyang 550025, PR China.*

*Corresponding author. Tel: +86 79183805183

E-mail: zhf19752003@163.com

ABSTRACT

A series of Cu(I) pyridyl-imidazole (PyIm) complexes with different aryl groups (Ar= naphthalene (**P2**), phenanthrene (**P3**), and anthracene (**P4**)) attached on the pyridyl ring are synthesized and characterized. The influence of these organic chromophore groups on the photophysical properties of the resulting complexes is investigated. Complexes **P2-P4** show stronger light harvesting efficiencies in the visible region compared with the parent complex **P1.** The emitting state of complex **P1** originates from the ^{3}MLCT state with some ^{3}LLCT character, while complexes **P2** and **P3** predominantly exhibit the ^{3}LLCT character. For complex **P4**, the triplet emitting state is dominated by the $^3(\pi\pi^*)$ state localized on the anthryl moiety, together with a lesser contribution form the ^{3}LLCT state. These changes in the photophysical properties were rationalized by DFT and TDDFT methods.

Keywords: Copper (I) complex; Pyridyl-imidazole; Molar extinction coefficient; Excited-state lifetime; Density functional theory

1. Introduction

Since the first dye-sensitized solar cells (DSSCs) employing a copper-based photosensitizer dye was reported in 1999 by Sauvage and coworkers [1], significant progresses have been made in the application of the Cu(I) complexes in DSSc in the recent years [2-10] due to their low cost and generally low toxicities. However, compared with power conversion efficiencies exceeding the value of 11% [11-14], there is still much room for improvement of the performance of the Cu(I)-based DSSCs [15] . Clearly, it is crucial to improve the light harvesting capability and increase excited-state lifetime of the Cu(I) complexes. In early study [16-18], Cu(I)-based dyes exhibit lower molar extinction coefficients (ε) on the order of 10^3 M^{-1} cm^{-1}, which means the poor light harvesting efficiency in DSSCs. To date, the molar extinction coefficients of the Cu(I)-based dyes have been increase to the order of 10^4 M^{-1} cm^{-1} by the judicious change of ligands [5,15], enabling greatly enhanced Cu(I)-based DSSC performance. Nonetheless, there is very little information available on the excited-state lifetime of such Cu(I)-based dyes in the reported literatures. It can be challenging to possess a high light harvesting efficiency while maintaining a long-lived lifetime for a successful Cu(I)-based photosensitizers.

Cu(I) complexes usually have the pseudo-tetrahedral coordination geometries in the ground state. However, these Cu(I) complexes readily undergo a severe Jahn-Teller distortion (flattening) upon excitation, which accelerates nonradiative decay of the emissive excited state, resulting in very short-lived lifetimes[19-21]. To prolong the excited-state lifetime, the generally accepted approach is to use the steric bulk of ligands to block geometrical distortion [22-25]. Especially, the most extensively studied class of complexes is four-coordinate heteroleptic Cu(I) species bearing a pyridyl azolate-based ligand together with a diphosphine ancillary ligand, exhibiting the higher quantum yields and long-lived lifetimes [26-29]. However, this types of complexes usually possess the poor light absorption in the visible region (ε), making them inferior toward DSSCs. Thus, further functionalizations of the ligands would open the possibility to design Cu(I)-based dyes with both high

light harvesting efficiencies and long-lived lifetimes. Combining organic chromophores with the parent complexes is an effective route to realize this goal. Herein, we present the synthesis, characterization, and photophysical properties of a series of the pyridyl-imidazole (PyIm) Cu(I) complexes containing naphthalene (naphthyl), phenanthrene (phenanthryl), and anthracene (anthryl) moieties (Figure 1, complexes **P2**-**P4**). We expect enhanced light absorption abilities to be provided by the addition of these light-harvesting groups while maintaining the long-lived excited state lifetimes. For comparison purpose, the parent Complex **P1** is also investigated as a reference. Additionally, the density functional theory (DFT) and time-dependent density functional theory (TDDFT) were employed to explain the photophysical properties.

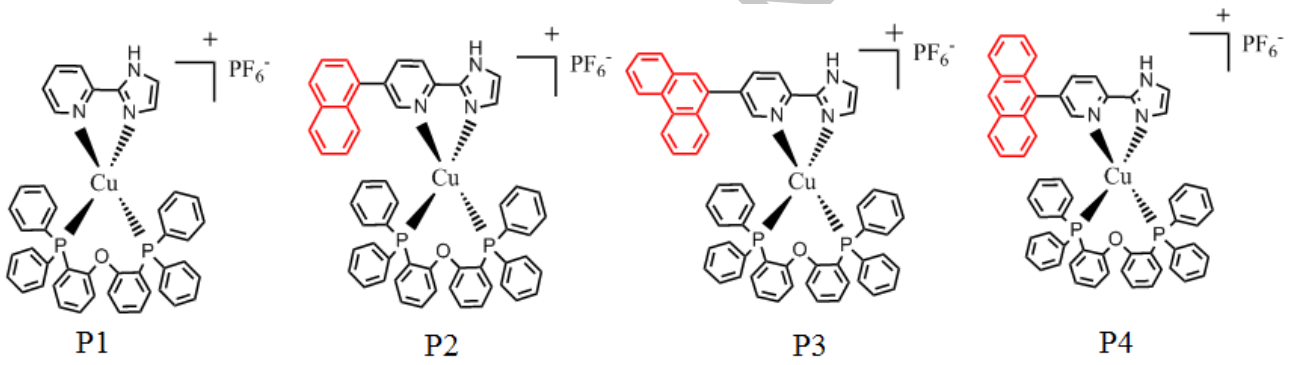

Figure 1

2. Experimental

2.1. Materials and methods

All reagents for synthesis were purchased from Sinopharm Chemical Reagent Co. Ltd. All the solvents for spectroscopic measurement were HPLC grade and were obtained from Vita-chemical Co. Ltd. and used without further purification. ^{1}H NMR spectra were performed in a Bruker AV400 MHz spectrometer, using tetramethylsilane (TMS) as internal reference. DMSO and $CDCl_3$ were used as the solvents. High-resolution mass spectra (HRMS) were obtained with the Agilent 6450 Q-TOF mass spectrometer using electrospray ionization (ESI). Elemental analyses of the complexes were carried out on an Elementar VarioEL cube analyzer. UV-vis absorption spectra were measured using a Perkin Elmer Lambda-900 spectrophotometer. Fluorescence spectra were determined with a Hitachi F-4600

fluorescence spectrophotometer. Photoluminescence (PL) quantum yields were determined using a Hamamatsu system for absolute PL quantum yield measurements (type C11347). Fluorescent lifetimes were measured with a compact fluorescent lifetime spectrometer (Hamamatsu, C11367, Japan).

2.2. Synthetic procedure

5-(naphthalen-1-yl)picolinaldehyde (2). ((5-bromopyridin-2-yl)methylene)oxonium (0.76 g, 4.08 mmol), Pd(PPh3)4 (0.38g, 0.33mmol) were added to a 20ml / 20ml anhydrous toluene / THF solution. Then, anhydrous ethanol 10 ml and 2 M K_2CO_3 solution (15 ml) dissolved in H_2O were added to the reaction mixture at 50 °C. Naphthalen-1-ylboronic acid (1.05 g, 6.12mmol) was added after half an hour and the mixture was refluxed for 5 h under nitrogen. After the reaction had finished, the mixture was filtered. The product was isolated using silica gel column chromatography with PE and EtAc (5:1) as the solvent. The solvent was removed by evaporation. Recrystallization of the residue from EtOH afforded a beige compound (0.94g, 4.03 mmol, 99% yield). ^{1}H NMR (400 MHz, DMSO) δ 10.12 (s, 1H), 8.96 (s, 1H), 8.19 (d, J = 2.0 Hz, 1H), 8.12 (s, 1H), 8.09 (d, J = 4.8 Hz, 2H), 7.77 (d, J = 8.3 Hz, 1H), 7.69 – 7.61 (m, 2H), 7.60 – 7.55 (m, 2H).

5-(phenanthren-9-yl)picolinaldehyde (3). This compound was prepared via a similar procedure for Compound **2** from ((5-bromopyridin-2-yl)methylene)oxonium (0.75g, 4.02 mmol) and phenanthren-9-ylboronic acid (1.33 g，6.03 mmol). The product was obtained as a pale yellow solid (1.06 g, 3.74 mmol, 93% yield). ^{1}H NMR (400 MHz, DMSO) δ 10.17 (s, 1H), 9.09 – 8.99 (m, 2H), 8.96 (d, *J* = 8.1 Hz, 1H), 8.31 (d, *J* = 7.8 Hz, 1H), 8.18 (d, *J* = 7.8 Hz, 1H), 8.11 (t, *J* = 10.7 Hz, 1H), 7.99 (s, 1H), 7.87 – 7.77 (m, 4H), 7.73 – 7.65 (m, 1H).

5-(anthracen-9-yl)picolinaldehyde (4). This compound was prepared via a similar procedure for Compound **2** from ((5-bromopyridin-2-yl)methylene)oxonium (0.77 g, 4.12 mmol), and anthracen-9-ylboronic acid (1.35g, 6.18 mmol). The product was obtained as yellow solid (0.98 g, 3.46 mmol, 62% yield). ^{1}H NMR (400 MHz, $CDCl_3$) δ 10.18 (s, 1H), 8.88 (s, 1H), 8.81 (s, 1H), 8.23 (s, 1H), 8.22 – 8.14 (m, 3H), 7.58 (d, *J* = 6.0 Hz, 2H), 7.50 (d, *J* = 13.2 Hz, 4H).

2-(1*H*-imidazol-2-yl)pyridine (L1). Anhydrous ethanol (25ml), Glyoxal solution (5ml) were

stirred in an ice bath, Then, picolinaldehyde (0.54 g, 5.02 mmol) and concentrated ammonia were added to the mixed solution under nitrogen for 1 h. The mixed solution was cooled to room temperature and allowed to stand for 12 h, extracted with dichloromethane and washed by water until neutral, and evaporated under reduced pressure to remove the solvent. The product was isolated using silica gel column chromatography with EtAc as the solvent. Recrystallization of the residue from EtOH afforded a brown compound (0.25 g, 1.72 mmol, 34% yield).^{1}H NMR (400 MHz, DMSO) δ 12.80 (s, 1H), 8.59 (d, J = 4.3 Hz, 1H), 8.04 (d, J = 7.9 Hz, 1H), 7.88 (t, J = 7.7 Hz, 1H), 7.39 – 7.31 (m, 1H), 7.15 (s, 2H).

2-(1*H*-imidazol-2-yl)-5-(naphthalen-1-yl) pyridine (L2). This compound was prepared via a similar procedure for **L1** from compound **2** (1.17g, 5.02 mmol) and concentrated ammonia were added to the mixed solution under nitrogen for 1 h. The mixed solution was cooled to room temperature and allowed to stand for 12 h, extracted with dichloromethan and washed by water until neutral, and evaporated under reduced pressure to remove the solvent.The product was isolated using silica gel column chromatography with EtAc as the solvent. Recrystallization of the residue from EtOH afforded a brown compound (0.44g, 1.62 mmol, 32% yield).^{1}H NMR (400 MHz, DMSO) δ 12.95 (s, 1H), 8.71 (s, 1H), 8.17 (t, J = 23.6 Hz, 1H), 8.05 (t, J = 7.3 Hz, 3H), 7.84 (d, J = 8.1 Hz, 1H), 7.67 – 7.55 (m, 4H), 7.22 (d, J = 56.0 Hz, 2H).

2-(1*H*-imidazol-2-yl)-5-(phenanthren-9-yl) pyridine (L3). This compound was prepared via a similar procedure for **L1** from compound **3** (1.44 g, 5.08 mmol), and Glyoxal solution (5ml). The product was obtained as yellow solid (0.52g, 1.62 mmol, 32% yield).^{1}H NMR (400 MHz, DMSO) δ 12.96 (s, 1H), 8.99 (d, J = 8.5 Hz, 1H), 8.92 (d, J = 7.8 Hz, 1H), 8.77 (s, 1H), 8.23 (d, J = 8.0 Hz, 1H), 8.13 – 8.06 (m, 2H), 7.93 (s, 1H), 7.85 (d, J = 8.2 Hz, 1H), 7.72 (ddd, J = 23.2, 13.9, 6.4 Hz, 4H), 7.28 (s, 2H)

5-(anthracen-9-yl)-2-(1H-imidazol-2-yl)pyridine (L4). This compound was prepared via a similar procedure for **L1** from compound **4** (1.17 g, 4.12 mmol), and Glyoxal solution (5ml). The product was obtained as yellow solid (0.35g, 1.09 mmol, 26% yield). ^{1}H NMR (400 MHz, DMSO) δ

13.02 (s, 1H), 8.77 (s, 1H), 8.62 (s, 1H), 8.31 (d, J = 8.0 Hz, 1H), 8.21 (d, J = 8.4 Hz, 2H), 7.99 (dd, J = 8.0, 1.8 Hz, 1H), 7.67 – 7.46 (m, 6H), 7.25 (s, 2H).

General procedure for preparation of PyIm-Cu(I) complexes. ImPy-Cu(I) complexes **P1-P4** were synthesized by the following route: $[Cu(CH_3CN)_4](PF_6)$ (0.124 g, 0.4mmol) and POP (0.216g, 0.4 mmol) reacted in dichloromethane (15 mL) at 25℃ for 2 h. Then, the corresponding PyIm ligand (0.4 mmol) was dissolved in the degassed dichloromethane solution and injected into the mixed solution for 2 h. The resulting mixture was filtered through a plug of Celite and concentrated to ca. 1 mL. Addition of Et_2O (10ml) to the filtrate afforded a pale yellow precipitate, which was collected and washed with Et_2O. And the product was recrystallized with ethanol.

[Cu(PyIm)(POP)](PF$_6$), **P1**. The product was a yellow powder (0.17g, 0.191 mmol, 48% yield). ^{1}H NMR (400 MHz, DMSO) δ 13.76 (s, 1H), 8.13 (s, 2H), 8.05 (s, 1H), 7.53 (s, 1H), 7.37 (d, J = 6.7 Hz, 8H), 7.28 (s, 11H), 7.12 (s, 2H), 7.08 (s, 2H), 7.06 (s, 1H), 7.04 (s, 1H), 6.96 – 6.78 (m, 3H), 6.66 (s, 2H). ^{13}C NMR (400 MHz, DMSO) δ 158.4 (s), 149.6 (s), 145.2 (s), 139.2 (s), 134.2 (s), 133.2 (s), 132.5 (s), 131.7 (s), 130.4 (s), 129.2 (s), 125.4 (s), 124.8 (s), 124.3 (s), 124.2 (s), 124.0 (s), 122.0 (s), 120.9 (s), 120.4 (s). HRMS (*m/z,* ESI$^+$): calcd. For $C_{44}H_{35}CuN_3OP_2$ ([M]$^+$) 746.1551; found 746.1530. Anal. Calcd. For $C_{44}H_{35}CuF_6N_3OP_3$ (892.23): C 59.23, H 3.95, N 4.71; found: C 59.61, H 4.02, N 4.53.

[Cu(Naph-PyIm)(POP)](PF$_6$), **P2**. The product was a brown powder (0.17g, 0.167 mmol, 42% yield). ^{1}H NMR (400 MHz, DMSO) δ 13.92 (s, 1H), 8.36 (s, 1H), 8.29 (s, 1H), 8.16 (s, 1H), 8.02 (s, 2H), 7.65 (s, 2H), 7.58 (s, 3H), 7.50 (s, 3H), 7.33 (s, 18H), 7.04 (s, 2H), 6.93 (s, 3H), 6.86 – 6.76 (m, 2H), 6.67 (s, 2H). ^{13}C NMR (100 MHz, DMSO) δ 157.7, 134.0 – 133.9, 133.6, 133.4 , 132.9 – 132.8, 131.9 , 130.1, 128.9, 128.7 , 128.5, 128.4, 128.2 – 128.0, 126.9 , 126.2 , 125.4 , 124.9 , 123.9 , 123.5 , 123.4– 123.3 , 120.2, 119.7. HRMS (m/z, ESI+): calcd. For $C_{54}H_{41}CuN_3OP_2$ ([M]+) 872.2021; found 872.2012. Anal. Calcd. For $C_{54}H_{41}CuF_6N_3OP_3$ (1018.38): C 63.69, H 4.06, N 4.13; found: C 63.38, H 4.27, N 4.43.

[Cu(Phen-PyIm)(POP)](PF$_6$), **P3**. The product was a pale yellow powder (0.18g, 0.168 mmol, 42% yield). ^{1}H NMR (400 MHz, DMSO) δ 13.91 (s, 1H), 8.74 (s, 1H), 8.43 (s, 1H), 8.17 (s, 2H), 8.15 (s, 2H), 7.63 (s, 1H), 7.55 (t, J = 7.2 Hz, 2H), 7.39 (s, 3H), 7.34 (s, 6H), 7.26 (s, 10H), 7.10 (s, 5H), 7.02 – 6.95 (m, 3H), 6.92 (s, 2H), 6.78 (d, J = 6.9 Hz, 2H), 6.68 (s, 2H). ^{13}C NMR (100 MHz, DMSO) δ 157.6 , 149.1 , 144.3, 144.1, 139.8, 136.1, 133.6, 132.7, 131.9, 130.4 , 130.0 , 129.7 , 129.1, 128.9 , 128.7, 128.6, 128.5 , 128.0, 127.6, 127.4 , 127.2, 127.1, 125.1, 124.9, 123.5, 122.9 , 121.60, 120.17 , 119.7. HRMS (m/z, ESI+): calcd. For $C_{58}H_{43}CuN_3OP_2$ ([M]+) 922.2177; found 922.2184. Anal. Calcd. For $C_{58}H_{43}CuF_6N_3OP_3$ (1068.44): C 65.20, H 4.06, N 3.93; found: C 65.71, H 4.42, N 3.50.

[Cu(Anthr-PyIm)(POP)](PF$_6$), **P4**. The product was a yellow powder (0.15 g, 0.140 mmol, 35% yield) . ^{1}H NMR (400 MHz, DMSO) δ 13.83 (s, 1H), 8.86 (d, *J* = 8.3 Hz, 1H), 8.81 (d, *J* = 8.2 Hz, 1H), 8.27 (d, *J* = 9.1 Hz, 2H), 8.10 (s, 1H), 7.87 (d, *J* = 6.7 Hz, 1H), 7.68 (t, *J* = 8.1 Hz, 4H), 7.57 (s, 1H), 7.41 (s, 3H), 7.25 (d, *J* = 7.2 Hz, 12H), 7.17 (s, 6H), 6.96 (t, *J* = 7.1 Hz, 3H), 6.81 (d, *J* = 6.7 Hz, 5H), 6.59 (s, 2H). ^{13}C NMR (100 MHz, DMSO) δ 157.7-157.5 , 150.3, 141.4-141.2 , 133.5, 133.2, 131.7, 130.6, 130.4 ,130.3, 129.9, 129.7,129.5, 128.9, 128.7 ,128.4, 128.2,128.0, 127.8, 127.4, 127.1, 126.5, 125.4 , 124.8, 123.6-123.42, 120.0, 119.6. HRMS (m/z, ESI+): calcd. For $C_{58}H_{43}CuN_3OP_2$ ([M]+) 922.2177; found 922.2165. Anal. Calcd. For $C_{58}H_{43}CuF_6N_3OP_3$ (1068.44): C 65.20, H 4.06, N 3.93; found: C 65.33, H 4.32, N 3.51.

2.3. DFT calculations

The B3LYP exchange-correlation function [30,31] was used to optimize the ground state (S_0 state) geometries of all the complexes using the polarized continuum model (PCM) [32] in CH_2Cl_2 media under the Gaussian 09 [33] program package. The 6-31G* basis set [34,35] was used for the C, H, N, O, and P atoms. The LANL2DZ basis set [36] was adopted for the Cu atom. On the basis of the optimized ground geometries, TDDFT method [37, 38] associated with PCM in CH_2Cl_2 media were used to simulate the absorption spectra of complexes studied. The first 200 singlet vertical excitations were obtained form the TDDFT output file to construct the calculated absorption spectra. Calculated

electronic density plots for the frontier molecular orbitals were prepared using Multiwfn analyzer soft [39] and VMD program [40].

3. Results and discussion

3.1. Synthesis

The synthetic pathways for the ligands and the corresponding Cu(I) complexes are shown in Scheme 1. Compounds **2-4** were synthesized by the straightforward cross-coupling reaction under standard Suzuki coupling condition [41]. The ligands **L1-L4** were prepared according to the literature procedure [42]. Complexes P**1-P4** were obtained by the conventional reactions of $[Cu(CH_3CN)_4]PF_6$ with one equivalent of the POP ligand and one equivalent of the corresponding ligands. The structures of these complexes were confirmed by ^{1}H NMR, HRMS and elemental analyses (see experimental section).

Scheme 1

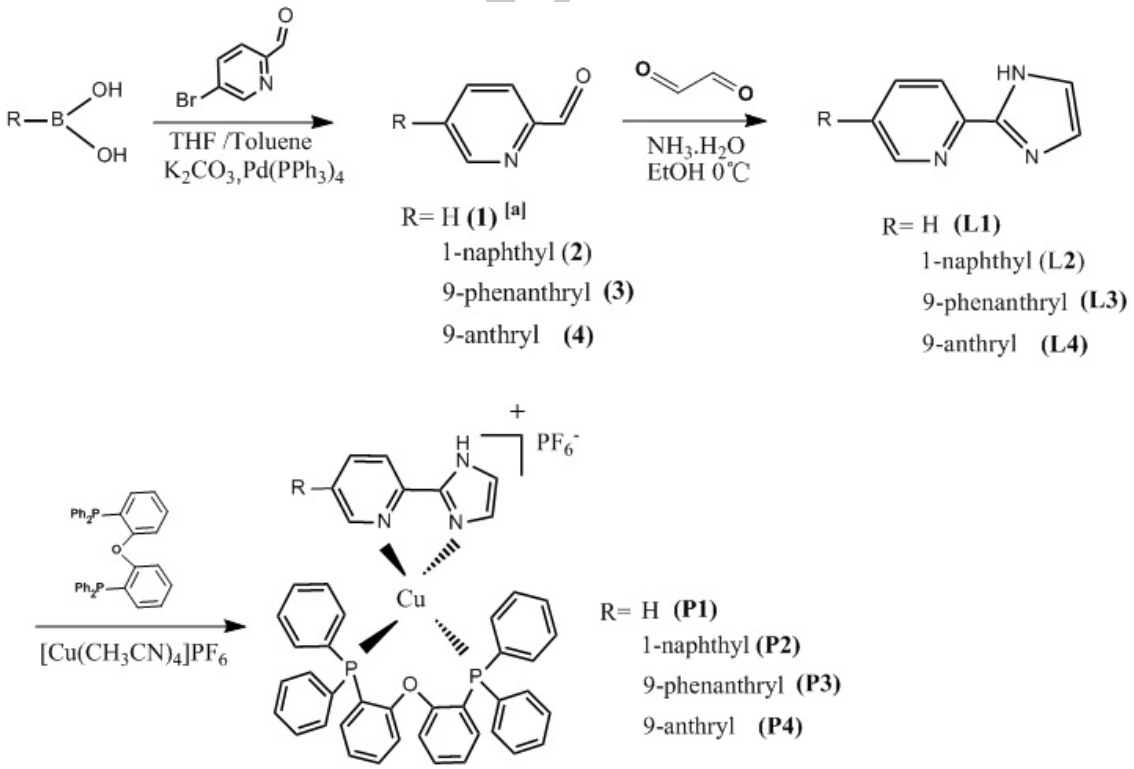

3.2. Photophysical properties

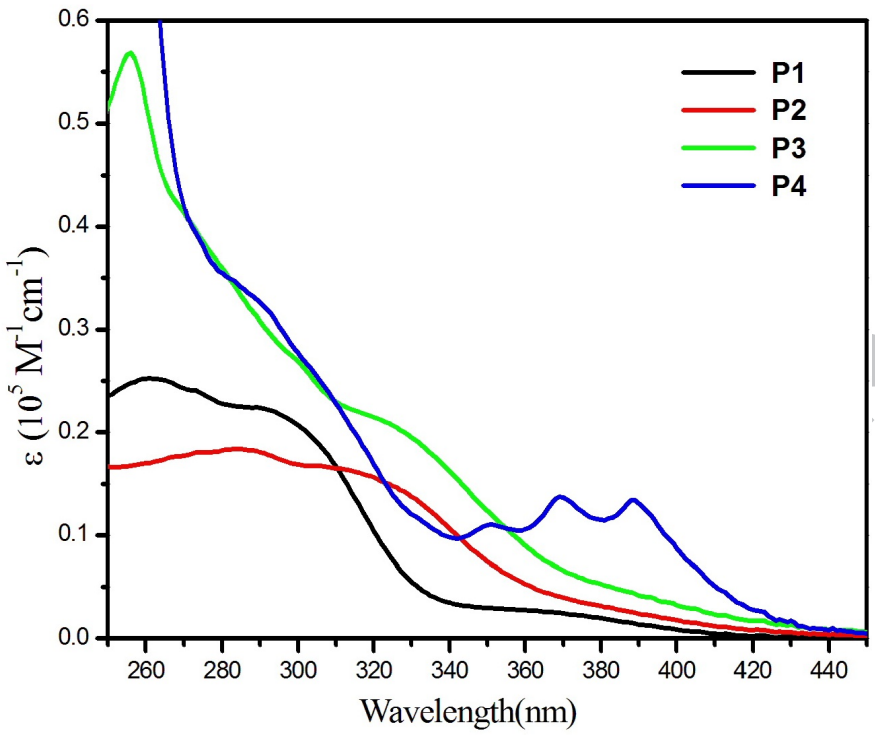

Figure 2

Table 1

	Absorption	Emission				
	λ_{abs} /nm ($\varepsilon \times 10^4$ M^{-1} cm^{-1})	λ_{em} /nm	τ/μs	Φ%	k_r/10^{4}s^{-1}	k_{nr}/10^{4}s^{-1}
P1	260 (2.5), 291 (2.2), 370 (0.24)	550	13.9	50.4	3.6	3.6
P2	284 (1.8), 319 (1.6), 370 (0.40)	578	58.6	10.5	0.18	1.5
P3	255 (5.7), 322 (2.1), 370 (0.67)	581	63.9	10.0	0.16	1.4
P4	285 (3.4), 350 (1.10), 370 (1.4), 388 (1.3)	548	12.8	10.0	0.78	7.0

UV-Vis spectra of the complexes **P1-P4** in CH_2Cl_2 solution at room temperature are shown in Figure 2 and the corresponding photophysical data are listed in Table 1. All these complexes exhibit intense bands ($\varepsilon > 1.6\times10^4$ M-1 cm^{-1}) in the region 250-340 nm assigned to $\pi\rightarrow\pi^*$ transitions involving both the PyIm and POP ligands. For the parent complex **P1**, the weaker and broader band between 340 and 420 nm (ε(370 nm) $\approx 2.4\times10^3$ M-1 cm^{-1}) is observed. This can be typically attributed to metal Cu to ligand charge transfer (MLCT) transition. The similar absorption transition (MLCT) can be observed for complexes **P2** and **P3** in the region of 360-420 nm. In case of complex **P4**, the MLCT transition can not be distinguished in low energy region, which is overlapped by the characteristic absorption band of anthryl group with three vibronic bands at 350, 370, and 388 nm. It is particularly noteworthy that complexes **P2-P4** with naphthyl, phenanthryl, and anthryl groups on the PyIm ligands,

respectively, significantly exhibit the enhanced light absorption abilities (ε(370 nm) ≈(4.0-6.7)×10^3 M^{-1} cm^{-1}) in the lower energy region compared to complex **P1,** which means that these chromophoric groups are potentially useful for improving light harvesting capacity of complexes.

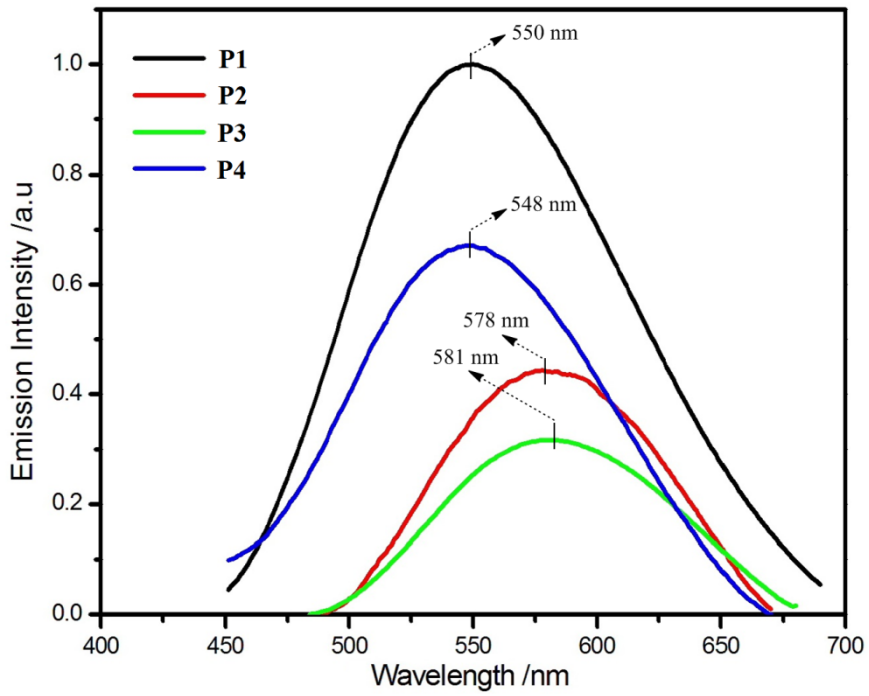

Figure 3

The emission spectra of **P1-P4** with the excitation wavelengths at 350, 340, 345 and 340 nm, respectively, at 298 K in PMMA films (10 wt %) are shown in Figure 3 and the corresponding parameters are also listed in Table 1. Comparing with emission of the free ligands (see Figure 1S, Supporting Information), the redshifts of the emission wavelength of the corresponding complexes are observed, suggesting that the emitting states of the complexes are triplet in nature. The parent complex **P1** displays a broad and structureless emission band centered at 550 nm, indicating that the emitting state originates from the lowest excited triplet state (T_1) with metal-to-ligand charge transfer (^{3}MLCT) character. The emission peaks of the complexes **P2** and **P3** centered at 578 and 581 nm, respectively, are red-shifted by 28-31 nm compared to that of the complex **P1** due to the increased πconjugation systems on the PyIm ligands. Despite the similarity in the emission spectral shapes of the complexes **P2** and **P3** with respect to complex **P1**, the luminescence lifetimes of the complexes **P2** and **P3** (τ=58.6

and 63.9 μs, respectively, see Figure 4) are much longer than that of the complex **P1** (τ=13.9 μs), thus suggesting that the emitting states of the complexes **P2** and **P3** have predominantly triplet ligand-to-ligand charge transfer (^{3}LLCT) character other than ^{3}MLCT character, as the long-lived emissions from the ^{3}LLCT state are usually observed [43]. In general, for the typical transition metal complexes, two types of the excited states contribute to the emission, namely, the ^{3}MLCT state and the ligand-centered (^{3}IL) state. Emission from a ^{3}MLCT state is commonly observed because this state typically lies lower in energy than the ^{3}IL state. However, the ^{3}IL state may become the lowest energy triplet state if the ligands are functionalized by organic groups with low triplet energy. Thus, the emission would be predominantly from the ^{3}LC state. Herein, the functionalization of the PyIm ligands with naphthyl and phenanthryl groups stabilizes the ^{3}LC state in a larger degree. As a consequence, the ^{3}LC state becomes the lowest emitting state. Based on the structural similarity compared to complexes **P2** and **P3**, it is to be expected that the emitting state of the complex **P4** has a ^{3}LLCT character. However, the slightly short lifetime (τ=12.8 μs) indicates that a mixed ^{3}LLCT and $^3(\pi\pi^*)$ character is more appropriate for complex **P4**. Further support for the assignments of these excited states is corroborated by the spin density distribution calculations (see below). Despite the presence of the stronger ππ stacking interaction caused by the larger π conjugation system in the ligands seems to somewhat compromise the emission quantum yields of the complexes **P2-P4** compared with complex **P1** (see Table 1), the introduction of organic chromophores into the parent Cu(I) complexes is still an efficient route for designing highly efficient Cu(I)-based dyes having both higher light absorption abilities and long-lived lifetimes.

Based on the known ϕ and τ values, the radiative rate constant (k_r) and nonradiative rate constant (k_{nr}) are calculated and summarized in Table 1. One can see that the values of k_r and k_{nr} are the same order of magnitude as those obtained in the literature [26, 27]. The k_r for complex **P1** is larger than that for complexes **P2-P4** by about 4-23-fold, leading to much higher ϕ value for complex **P1**. The values of k_r and k_{nr} for complexes **P2** and **P3** are almost identical, whereas the values of k_r and k_{nr} of the complex

P4 are larger by 4-5 times than those of **P2** and **P3**. The change in k_r and k_{nr} values suggests a change of the character of the emitting transition on going from complex **P1** to **P4**, which are in line with the assignments of the emitting states as mentioned above.

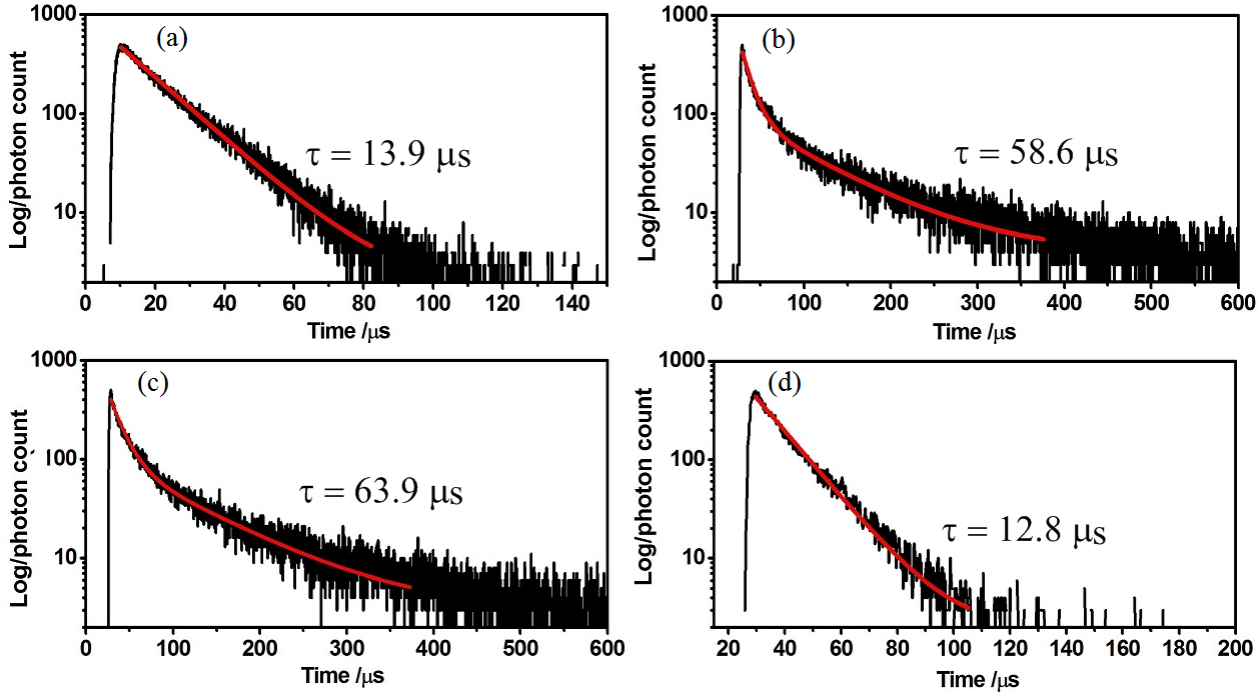

Figure 4

3.3. Theoretical calculations

Based the optimized ground geometries of the complexes **P1-P4** in CH_2Cl_2 solution at the B3LYP/6-31G(d)/LANL2DZ levels of theory, the energy levels, atomic orbital compositions, and energy gaps of the HOMO and LUMO of the complexes are shown Figure 5. For the parent complex **P1**, the highest occupied molecular orbital (HOMO) is localized on the metal Cu atom and POP ligand, while the lowest unoccupied molecular orbital (LUMO) mainly distributes on the pyridyl ring. Therefore, the functionalization of the pyridyl ring would have a significantly influence on the LUMO level. Here, the induction of naphthyl and phenanthryl groups into the pyridyl ring extends the whole π conjugation system of the pyridyl-imizole ligand, giving a decrease of the LUMO energy level. As expected, the LUMO energy levels of the complexes **P2** and **P3** are calculated to be -2.15 and -2.17 eV lower than complex **P1** (-2.02 eV), respectively, while the HOMO energy levels of the complexes **P1**-

P3 remain almost unchanged. Unlike complexes **P1-P3**, the HOMO and LUMO of the complex **P4** are mainly distributed on the anthryl group. The HOMO energy is calculated to be -5.59 eV, which is less stable than those of the complexes **P1-P3**. The LUMO energy (-2.21 eV) is calculated to be more stable compared to **P1** and **P2**. The HOMO-LUMO energy gap can be obtained in the order **P1** (3.96 eV) > **P2** (3.84 eV) > **P3** (3.82 eV) > **P4** (3.38 eV), which is consistent with the absorption onset in low energy region observed in the experiment spectra.

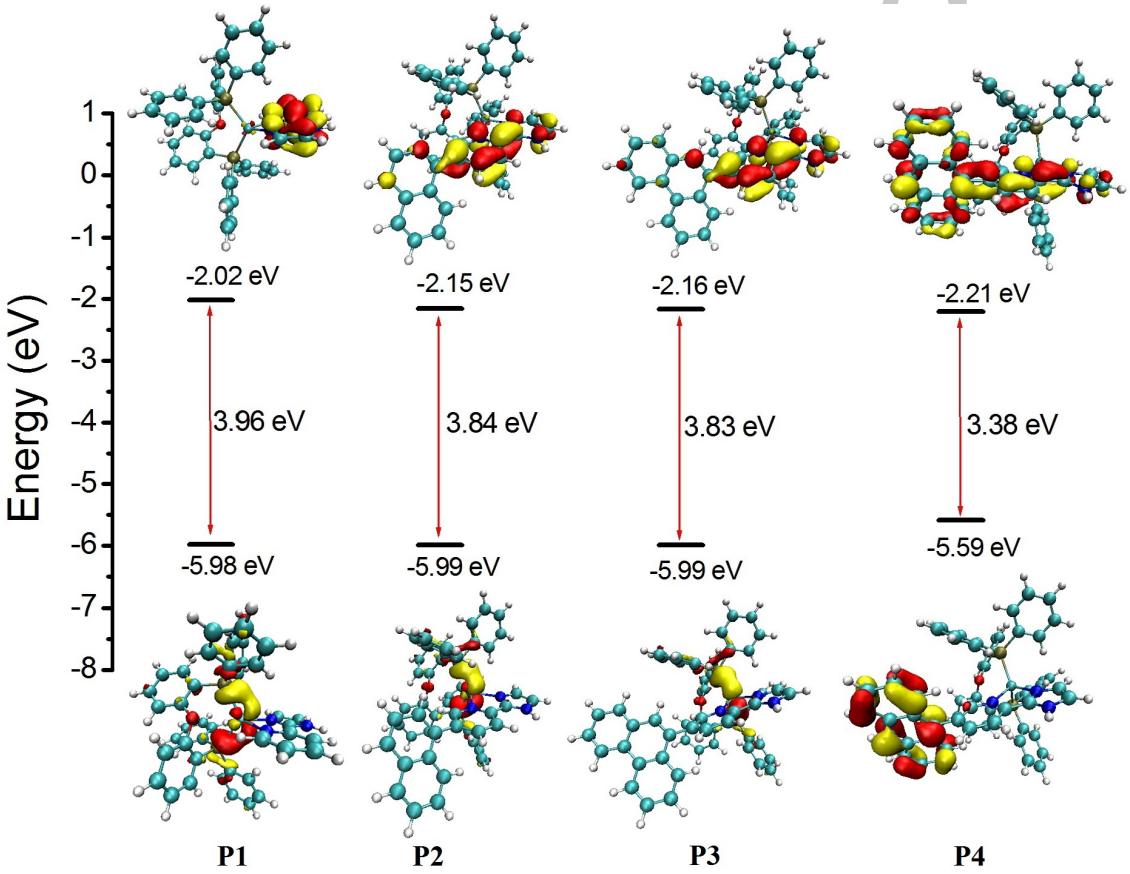

Figure 5

Table 2 (see the attached files)

The calculated spectra of the complexes **P1-P4** employing TDDFT method in CH_2Cl_2 solution are shown in Figure 6, together with the experimental spectra for comparison purpose. Table 2 shows the relative molecular orbital and transition characters (see the detailed information in Figure 2S, Table 1S-4S in the Supporting Information). The calculated spectra reproduced nicely the shapes and positions of the experimental spectra. For complex **P1**, the first lowest excited state S_1, calculated at 374 nm, mainly composed of HOMO→LUMO transition, is in good agreement with the experimental

shoulder centered at about 370 nm. A composition analysis of the HOMO and LUMO (see Table 1S, Supporting Information) clearly shows that this excitation can be ascribed as MLCT/LLCT character, supporting the original assignment of the absorption bands in the experiment. The experimental absorption bands in the region of 250-320 nm are mainly originated from the combination transitions of the S_6, S_7, S_{11}, S_{15}, S_{19} and S_{28} states with the ($\pi\pi^*$) transition character within both POP and PyIm ligands but mixed with little contribution of MLCT/LLCT transition (see Table 2). For complex **P2**, the experimental shoulder at λ>340 nm appears to be composed of the S_1, S_2, and S_3 with the calculated peaks at 353, 365, and 384 nm, respectively, showing primary LLCT character from the S_2 state since the oscillator strength of this transition is largest (f=0.1560), with the mixing of some MLCT character originated from the S_1 and S_3 states. The calculated absorption bands in the range 260-340 nm are dominated by the mixed transitions of the S_6, S_8, S_{10}, and S_{13} states with the transition character of ($\pi\pi^*$)/LLCT. For complex **P3,** the S_1, S_2, and S_3 states, calculated at 355, 368, and 385 nm, respectively, are responsible for the experimental shoulder at λ>360 nm with LLCT/MLCT character. The two intense transitions at 313 and 305 nm, originating from the S_7 and S_9, respectively, appear to give rise to the 310-360 nm shoulder of the experimental spectrum with ($\pi\pi^*$)/LLCT character. An intense band calculated at 248 nm, originating from the S_{67} state, can be related to the absorption peak experimentally found at 260 nm with ($\pi\pi^*$)/LLCT character. With respect to complex **P4**, the characteristic absorption bands of the anthryl moiety in the range of 340 -400 nm in the experimental spectrum are reflected by the calculated two absorption bands at 394 and 428 nm from the S_1 and S_2 states, respectively, which are originated from the starting orbitals of the HOMO [π(Anth)] to the arriving orbitals of LUMO/LUMO+1[π^*(Anth)] with ($\pi\pi^*$) character. It is noteworthy that the S_3 state calculated at 384 nm with MLCT/LLCT character has a comparative contribution to this experimental shoulder, which is not well distinguished in the experimental spectrum. The weak shoulder experimentally found in the range 270-320 nm is composed of a series of lower intensity transitions, dominated by the S_{11}, S_{12}, S_{13}, S_{17}, S_{19}, S_{20} and S_{25} (see inset of Figure 6d). These

transitions have ($\pi\pi^*$)/LLCT/MLCT character, originating from the starting orbitals of the HOMO-1/HOMO-2/HOMO-4 combinations to the arriving orbitals of LUMO/LUMO+1/LUMO+3/LUMO+4/LUMO+5/LUMO+6. A very intense band calculated at 248 nm originated from the S_{80} state is assigned as ($\pi\pi^*$)/LLCT character, which is related to the 256 nm band of the experimental spectrum. Notably, this 256 nm absorption band exhibits the oscillator strength as high as 1.3140, which is also reflected by a very high ε value of 142 500 M^{-1} cm^{-1} in the experiment.

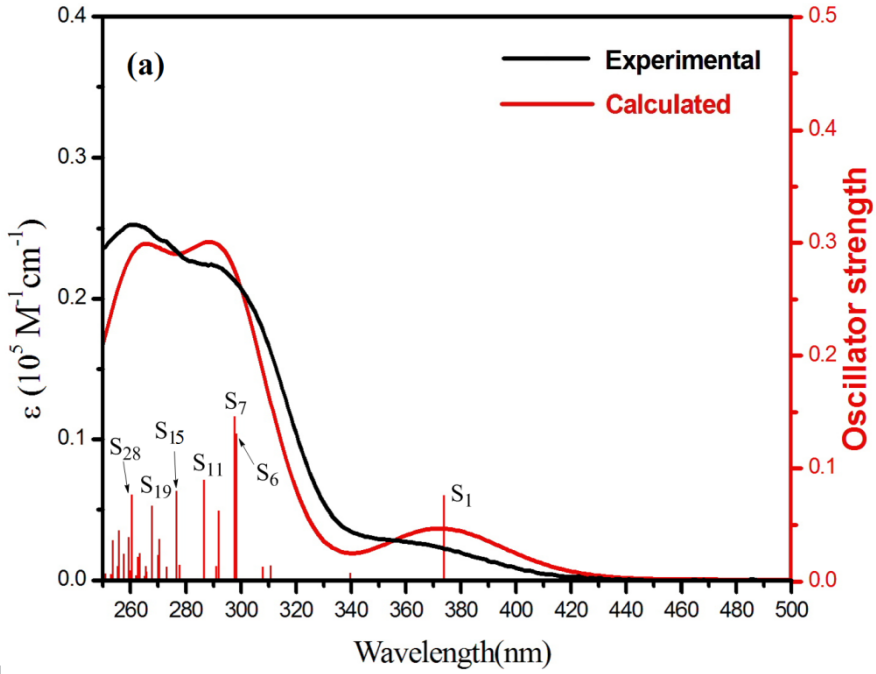

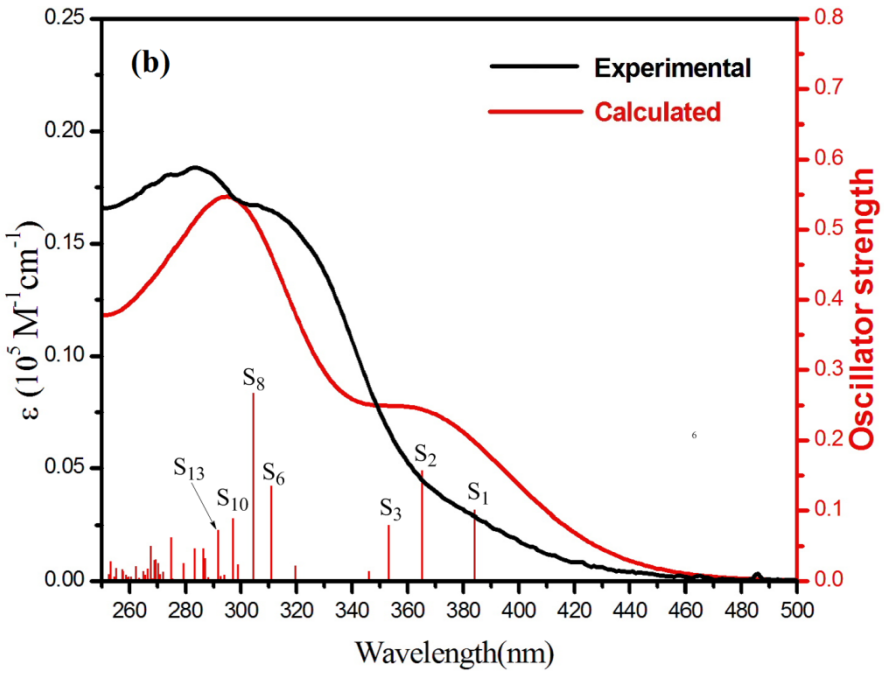

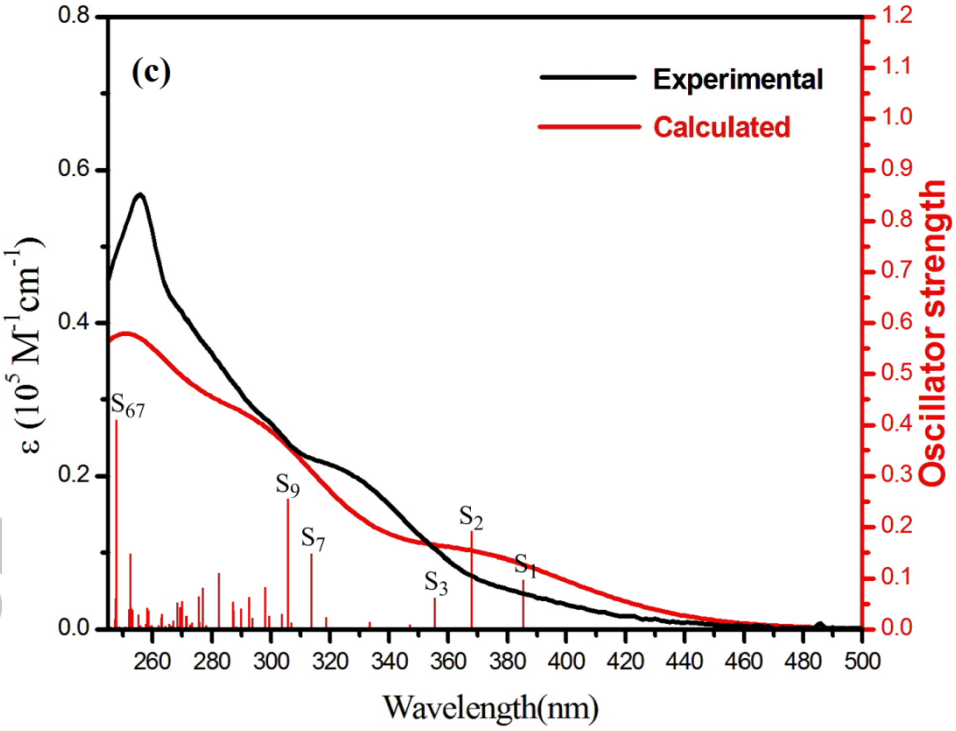

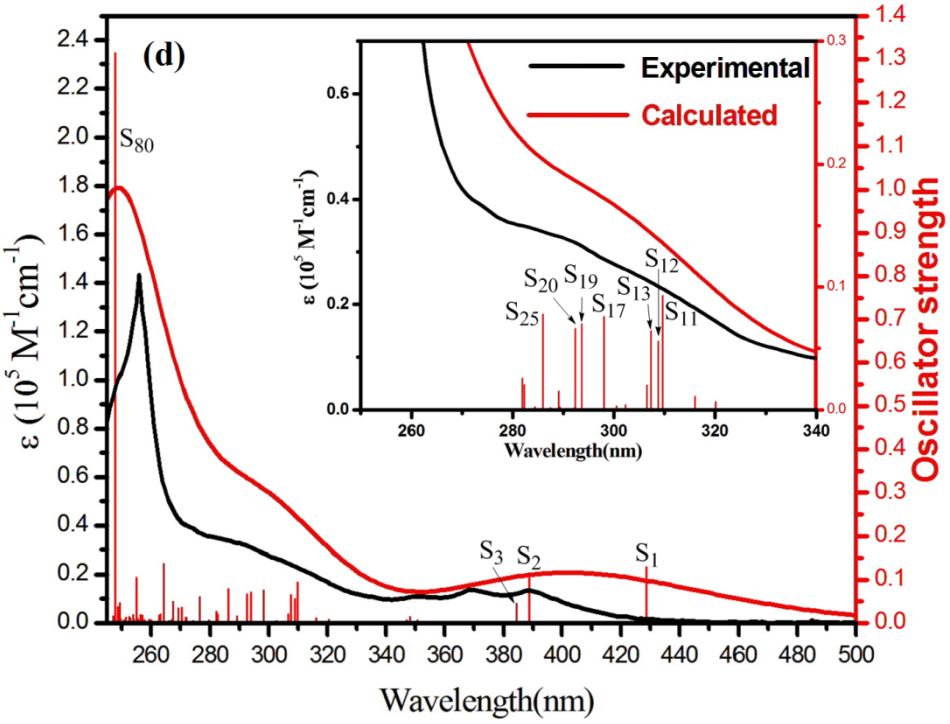

Figure 6

To gain further understanding of the nature of the triplet emitting states, the triplet excited state geometries of the complexes **P1-P4** were optimized using the spin-unrestricted U-DFT approach, imposing a spin multiplicity of **3**. The calculated emission energy based on ΔSCF method [44] was calculated to be 1.96, 1.82 and 1.83 eV, for complexes **1-3**, respectively, which is in reasonably good agreement with the corresponding experimental values (2.25, 2.15 and 2.13 eV) with exception of the complex **4** that its calculated emission energy (1.41 eV) was considerably lower than the experimental value (2.26 eV). The large discrepancy between calculated and experimental values for complex **4** might be partly explained by the large the structural relaxation of the excited state. Figure 7 displays the spin density distributions of all the complexes based on the optimized lowest triplet state geometry. For the parent complex **P1**, the unpaired electron spin-density distributions in the T_1 state (Cu, 0.54e; POP, 0.32e; PyIm, 1.15e) clearly illustrates the higher contribution of the d(Cu) to the PyIm ligand with some contribution of POP ligand to the PyIm ligand and confirm the emission behavior of ^{3}MLCT/^{3}LLCT character. The emitting state of the complexes **P2** and **P3** undoubtedly can be assigned as the ^{3}LLCT character with PyIm →Naph transition for **P2**, PyIm →Phen transition for **P3**, which is also

supported by the spin-density distributions in T_1 state (Cu, 0.005e; POP, 0.003e; PyIm, 0.79e; Naph, 1.30e for **P2**; Cu, 0.006e; POP, 0.003e; PyIm, 0.72e; Phen, 1.26e for **P3**). With respect to complex **P4**, the unpaired electrons in T_1 state are dominantly localized on anthryl group with a small contribution from the PyIm ligand (Cu, 0.002e; POP, 0.002e; PyIm, 0.28e; Anth, 1.82e), indicating that the emitting state of the complex **P4** has a ^{3}LC $\pi\pi^*$ character with a ^{3}LLCT contribution from the PyIm ligand to anthryl group. These theoretical results further support the assignments of the nature of the emitting excited state.

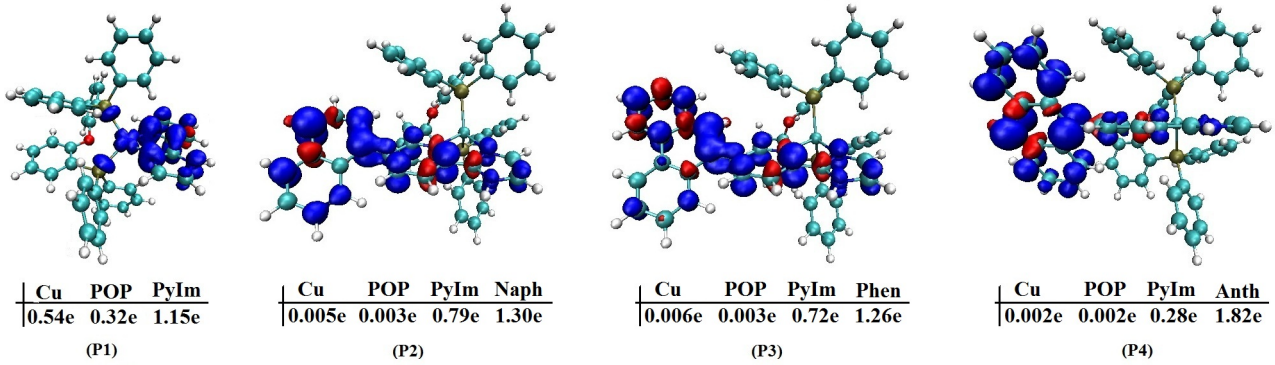

Figure 7

4. Conclusion

In summary, Cu(I) complexes containing the pyridyl-imidazole (PyIm) ligand functionalized by the different organic chromophores have been synthesized and characterized. Complexes **P2-P4** exhibit the enhanced light absorption ability in the visible region compared with the parent complex **P1** with the long-lived excited state lifetimes, which are potentially useful for the harvesting of solar energy. The emitting state of the complexes can be altered from the ^{3}MLCT/^{3}LLCT state (complex **P1**) to the ^{3}LLCT state (complexes **P2** and **P3**) to the $^3(\pi\pi^*)$/^{3}LLCT state (complex **P4**) by modulating the orbital energy levels of the ligands. These structure-property relationships are further rationalized by DFT and TDDFT calculations.

Acknowledgements. The work was supported by the National Natural Science Foundation of China (No. 21563013) and the Natural Science Foundation of Jiangxi Province (No. 20151BAB203006).

The authors thank the Guizhou University High Performance Computation Chemistry Laboratory (GHPCC) for help with computational studies.

References

[1]. N. Alonso-Vante, J.F. Nierengarten, J.P. Sauvage, J. Chem. Soc. Dalton Trans. (1994) 1649-1654.
[2]. B. Bozic-Weber, S.Y. Brauchli, E.C. Constable, S.O. Furer, C.E. Housecroft, I.A. Wright, Phys. Chem. Chem. Phys. 15 (2013) 4500-4504.
[3]. B. Bozic-Weber, S.Y. Brauchli, E.C. Constable, S.O. Furer, C.E. Housecroft, F.J. Malzner, I.A. Wright, J.A. Zampese, Dalton. Trans., 42 (2013) 12293-12308.
[4]. T.E. Hewat, L.J. Yellowlees, N. Robertson, Dalton. Trans., 43 (2014) 4127-4136.
[5]. K.A. Wills, H.J. Mandujano-Ramirez, G. Merino, D. Mattia, T. Hewat, N. Robertson, G. Oskam, M.D. Jones, S.E. Lewis, P. J. Cameron, RSC Adv, 3(2013) 23361-23369.
[6]. F.J, Malznerm S.Y. Brauchli, E.C. Constable, C.E. Housecroft, M. Neuburger, RSC Adv., 4 (2014) 48712-48723.
[7]. C.E. Housecroft, E.C. Constable, Chem. Soc. Rev., 44 (2015) 8386-8398.
[8]. S.O. Furer, B. Bozic-Weber, M. Neuburger, E.C. Constable, C.E. Housecroft, RSC Adv., 5 (2015) 69430-69440.
[9]. Y. Maximilian Klein, M. Willgert, A. Prescimone, E.C. Constable, C.E. Housecroft, Dalton Trans., 45 (2016) 4659-4672.
[10]. F.J. Malzner, A. Prescimone, E.C. Constable, C.E. Housecroft, M. Willgert, J. Mater. Chem. A., 5 (2017) 4671-4685.
[11]. C.Y. Chen, M.K. Wang, J.Y. Li, N. Pootrakulchote, L. Alibabaei, C. Ngoc-le, J.D. Decoppet, J.H. Tsai, C. Gratzel, C.G. Wu, S.M. Zakeeruddin, M. Gratzel, ACS Nano., 3 (2009) 3103.
[12]. L.L. Li, E.W.G. Diau, Chem. Soc. Rev., 42 (2013) 291.
[13]. K. Kakiage, Y. Aoyama, T. Yano, T. Otsuka, T. Kyomen, M. Unno, M. Hanaya, Chem. Comm., 50 (2014) 6379-6381.
[14]. C.C. Chou, F.C. Hu, H.H. Yeh, H.P. Wu, Y. Chi, J.N. Clifford, E. Palomares, S.H. Liu, P.T. Chou, G.H. Lee, Ange. Chem. Inter. Ed., 53 (2014) 178-183.
[15]. M. Sandroni, L. Favereau, A. Planchat, H. Akdas-Kilig, N. Szuwarski, Y. Pellegrin, E. Blart, H.L. Bozec, M. Boujtita, F. Odobel, J. Mater. Chem. A. 2 (2014) 9944-9947.
[16]. S. Sakaki, T. Kuroki, T. Hamada, J. Chem. Soc. Dalton. Trans., (2002) 840-842.
[17]. T. Bessho, E.C. Constable, M. Graetzel, A.H. Redondo, C.E. Housecroft, W. Kylberg, M.K. Nazeeruddin, M. Neuburger, S. Schaffner, Chem. Commun., (2008) 3717-3719.
[18]. C.L. Linfoot, P. Richardson, T.E. Hewat, O. Moudam, M.M. Forde, A. Collins, F. White, N. Robertson, Dalton. Trans., 39 (2010) 8945-8956.
[19]. A. Lavie-Cambot, M. Cantuel, Y. Leydet, G. Jonusauskas, D.M. Bassani, N.D. McClenaghan, Coord. Chem. Rev., 252 (2008) 2572-2584.
[20]. D.V. Scaltrito, D.W. Thompson, J.A. O'Callaghan, G.J. Meyer, Coord. Chem. Rev., 208 (2000) 243-266.
[21]. G.B. Shaw, C.D. Grant, H. Shirota, E.W. Castner, G.J. Meyer, L.X. Chen, J. Am. Chem. Soc., 129 (2007) 2147-2160.
[22]. D.G. Cuttell, S.M. Kuang, P.E. Fanwick, D.R. McMillin, R.A. Walton, J. Am. Chem. Soc., 124 (2002) 6-7.
[23]. K.Saito, T. Arai, N. Takahashi, T. Tsukuda, T. Tsubomura, Dalton. Trans., (2006) 4444-4448.

[24]. P. Aslanidis, P.J. Cox, A.C. Tsipis, Dalton. Trans., 39 (2010) 10238-10248.
[25]. G. Accorsi, N. Armaroli, C. Duhayon, A. Saquet, B. Delavaux-Nicot, R. Welter, O. Moudam, M. Holler, J.F. Nierengarten, Eur. J. Inorg. Chem., 2010 (2010) 164-173.
[26]. C.W. Hsu, C.C. Lin, M.W. Chung. Y. Chi, G.H. Lee, P.T. Chou, C.H. Chang, P.Y. Chen, J. Am. Chem. Soc., 133 (2011) 12085.
[27]. A. Wada, Q.S. Zhang, T. Yasuda, I. Takasu, S. Enomoto, C. Adachi, Chem. Comm., 48 (2012) 5340-5342.
[28]. L. Bergmann, J. Friedrichs, M. Mydlak, T. Baumann, M. Nieger, S. Brase, Chem. Comm., 49 (2013) 6501-6503.
[29]. X.L. Chen, R.M. Yu, Q.K. Zhang, L.J. Zhou, X.Y. Wu, Q. Zhang, C.Z. Lu, Chem. Mater., 25 (2013) 3910-3920.
[30]. E. Runge, E. K. Gross, Phys. Rev. Lett. 52 (1984) 997.
[31]. S. L. Mayo, B. D. Olafson, W. A. Goddard, J. Phys. Chem. 94 (1990) 8897.
[32]. J. P. Perdew, K. Burke, M. Ernzerhof, Phys. Rev. Lett. 78 (1997) 1396
[33]. M. J. Frisch, G. W. Trucks, H. B. Schlegel, G. E. Scuseria, M. A. Robb, J. R. Cheeseman, J. A. Montgomery, Jr.,T. Vreven, K. N. Kudin, J. C. Burant, J. M. Millam, S. S. Iyengar, J. Tomasi, V. Barone, B. Mennucci, M. Cossi, G. Scalmani, N. Rega, G. A. Petersson, H. Nakatsuji, M. Hada, M. Ehara, K. Toyota, R. Fukuda, J. Hasegawa, M. Ishida, T. Nakajima, Y. Honda, O. Kitao, H. Nakai, M. Klene, X. Li, J. E. Knox, H. P. Hratchian, J. B. Cross, C. Adamo, J. Jaramillo, R. Gomperts, R. E. Stratmann, O. Yazyev, A. J. Austin, R. Cammi, C. Pomelli, J. W. Ochterski, P. Y. Ayala, K. Morokuma, G. A. Voth, P. Salvador, J. J. Dannenberg, V. G. Zakrzewski, S. Dapprich, A. D. Daniels, M. C. Strain, O. Farkas, D. K. Malick, A. D. Rabuck, K. Raghavachari, J. B. Foresman, J. V. Ortiz, Q. Cui, A. G. Baboul, S. Clifford, J. Cioslowski, B. B. Stefanov, G. Liu, A. Liashenko, P. Piskorz, I. Komaromi, R. L. Martin, D. J. Fox, T. Keith, M. A. AlLaham, C. Y. Peng, A. Nanayakkara, M. Challacombe, P. M. W. Gill, B. Johnson, W. Chen, M. W. Wong, C. Gonzalez, J. A. Pople, GAUSSIAN09, Revison A 02, Gaussian Inc., Pittsburgh, PA, 2009.
[34]. P. C. Hariharan, J. A. Pople, Mol. Phys. 27 (1974) 209.
[35]. M. S. Gordon, Chem. Phys. Lett. 76 (1980) 163.
[36]. P.J. Hay, W.R. Wadt, J. Chem. Phys. 82 (1985) 270.
[37]. M.E. Casida, C. Jamorski, K.C. Casida, D.R. Salahub, J. Chem. Phys. 108 (1998) 4439.
[38]. R.E. Stratmann, G.E. Scuseria, M.J. Frisch, (1998) J. Chem. Phys. 109 (1998) 8218.
[39]. T. Lu, F. W. Chen, J. Comput. Chem. 33 (2012) 580.
[40]. W. Humphrey, A. Dalke, K. Schulten, J. Mol. Graphics. 14 (1996) 33.
[41]. N. Miyaura, A. Suzuki, Chem. Rev., 95 (1995) 2457-2483.
[42]. Q.M. Wang, H. Tamiaki, J. Photochem. Photobiol. A., 206 (2009) 124.
[43]. J.L. Chen, X.F. Cao, J.Y. Wang, L.H. He, Z.Y. Liu, H.R. Wen, Z.N. Chen, Inorg. Chem., 52 (2013) 9727-9740.
[44]. T. Kowalczyk, S.R. Yost, T. Van Hooris, J. Chem. Phys., 134 (2011) 054128.

Figure Captions

Figure 1. Molecular structures of Cu(I) complexes containing different aryl groups in this study.

Scheme 1. The synthetic pathways of the PyIm derivatives and the resulting Cu(I) complexes. [a] Purchased from market.

Figure 2. Absorption spectra in dichloromethane (C=1×10^{-5} mol/L) at 298K of complexes **P1-P4**.

Figure 3. Normalized emission spectra of complexes **P1-P4** in PMMA films (10wt%).

Figure 4. Emission decay curves in PMMA films (10wt%) at 298 K for **P1** (a), **P2** (b), **P3** (c), **P4** (d). Red solid lines drawn through the data points correspond to the best exponential fitting. Excitation wavelength =370 nm, emission monitored at 550, 580, 582, and 545 nm for **P1-P4**, respectively.

Figure 5. The energy levels and atomic orbital compositions calculated for the HOMO and LUMO of complexes **P1-P4.**

Figure 6. Comparison of the calculated (red line) and experimental (black line) absorption spectra in CH_2Cl_2 solution for **P1** (a), **P2** (b), **P3** (c), and **P4** (d). Red vertical lines correspond to oscillator strength of calculated singlet-singlet transitions.

Figure 7. Spin density distribution contours (isovalue = 0.004) for the lowest triplet state T_1 of complexes **P1-P4**. The values of the unpaired-electron spin-density population are depicted together with the electronic nature of the states.

Table captions

Table 1. Photophysical properties of complexes **P1-P4.**

Table 2. Electronic absorptions of complexes **P1-P4** in CH_2Cl_2 based on TDDFT calculations at the (B3LYP)/6-31g*/LANL2DZ level, together with the experimental values.